Multiscale Model. Simul.
Vol. 12, No. 3, pp. 1379–1400
© 2014 Society for Industrial and Applied Mathematics

Downloaded 02/26/15 to 124.16.148.3. Redistribution subject to SIAM license or copyright; see http://www.siam.org/journals/ojsa.php

A STUDY ON THE QUASI-CONTINUUM APPROXIMATIONS OF A ONE-DIMENSIONAL FRACTURE MODEL*

XIANTAO LI† AND PINGBING MING‡

Abstract. We study three quasi-continuum approximations of a lattice model for crack propagation. The influence of the approximation on the bifurcation patterns is investigated. The estimate of the modeling error is applicable to near and beyond bifurcation points, which enables us to evaluate the approximation over a finite range of loading and multiple mechanical equilibria.

Key words. quasi-continuum methods, bifurcation analysis, ghost force, lattice fracture model

AMS subject classifications. 65N15, 74G15, 70E55

DOI. 10.1137/130939547

1. Introduction.

In recent years multiscale models have undoubtedly become one of the most important computational tools for problems in materials science. Such multiscale models allow atomistic details of local defects, while taking advantage of the efficiency of continuum models in handling the calculations in the majority of the computational domain. One remarkable success in multiscale modeling of materials science is the quasi-continuum (QC) method [42], which couples a molecular mechanics model with a continuum finite element model. The QC method has motivated a lot of recent works on multiscale models of crystalline solids [21, 1, 44, 40, 22].

Meanwhile, there has been considerable interest from the applied mathematics community to analyze the stability and accuracy of QC-type methods [26, 16, 15, 30, 31, 10, 11, 14, 39, 5, 33, 32, 9, 27, 25]. Various important issues, such as the ghost forces and stability, have been extensively investigated. One major weakness of all the existing results, however, is that they are only applicable to a system near *one* local minimum with a fixed load. This significantly limits the practical values of these analyses. First, for any given loading condition, there are typically a large number of local mechanical equilibria, even for a relatively simple system [20]. Second, often of interest in practice is the transition of the system as the loading condition changes. Examples include phase transformation [17], crack propagation and kinking [6, 8], dislocation nucleation [36], etc. Throughout these processes, the system is driven from a stable equilibrium to a critical point, where the system loses its stability, and then settles to another equilibrium.

Fortunately, the theory of bifurcation [41, 4, 19, 2, 7, 28] provides a rigorous tool for understanding the transition processes. The theory considers models, either static or dynamic, with certain embedded parameters, which for mechanics problems naturally correspond to the external loading conditions. Bifurcation arises when the

*Received by the editors October 2, 2013; accepted for publication (in revised form) June 24, 2014; published electronically September 30, 2014.
http://www.siam.org/journals/mms/12-3/93954.html

†Department of Mathematics, The Pennsylvania State University, University Park, PA 16802 (xli@math.psu.edu). The work of this author was supported by National Natural Science Foundation grant DMS1016582.

‡LSEC, Institute of Computational Mathematics and Scientific/Engineering Computing, AMSS, Chinese Academy of Sciences, Beijing 100190, China (mpb@lsec.cc.ac.cn). The work of this author was supported by National Natural Science Foundation of China grant 91230203, funds from Creative Research Groups of China through grant 11321061, and the CAS National Center for Mathematics and Interdisciplinary Sciences.

Copyright © by SIAM. Unauthorized reproduction of this article is prohibited.

Downloaded 02/26/15 to 124.16.148.3. Redistribution subject to SIAM license or copyright; see http://www.siam.org/journals/ojsa.php

system loses its stability, and it is a ubiquitous phenomenon in mechanics [29]. A reduction procedure is available [4] to probe the transition process. Of particular interest in this context is the bifurcation diagram, consisting of bifurcation curves for a wide range of parameters. The curves contain local equilibria, including both stable and unstable ones. As a result, the analysis is well beyond local stable equilibria. This is the primary motivation for the current work.

The molecular mechanics model becomes highly indefinite at the bifurcation point, and the standard analysis is not applicable due to the loss of coercivity. In fact, most existing results relied on even more strict stability conditions. We refer the reader to [16, 31, 11, 14] for related discussion. There are some methods that have sharp stability conditions [13, 27]. It is also worthwhile to mention that there are some interesting works that quantify the error of the atomistic/continuum coupling methods up to the bifurcation, as well as those that estimate the error of the critical loads. We refer the reader to [12, 34] and the references therein. Nevertheless, these analyses do not predict the modeling error beyond the bifurcation point.

The aim of this paper is to evaluate the modeling error associated with multiscale coupling methods. In order to be able to precisely quantify the error, we consider a one-dimensional fracture model, which is sophisticated enough to model some aspects of fracture mechanics and, in the meantime, simple enough so that direct mathematical calculations are amenable. We have chosen to analyze three multiscale methods, including the original QC method, the quasi-nonlocal method, and a force-based method. They represent three major types of methods: energy-based methods with ghost forces, energy-based methods without ghost forces, and force-based methods without an associated energy, respectively. A novel aspect of our analysis is that it is applicable to a wide range of loading conditions, during which the system may go through bifurcations and experience stability transition. In particular, the one-dimensional model exhibits a saddle-node bifurcation with two intrinsic parameters, which in turn determine the bifurcation curve. It has been found that the original QC method, with the notorious problem of ghost forces, exhibits large error in predicting the bifurcation curve. The quasi-nonlocal QC method and the force-based method, on the other hand, are quite accurate in this aspect. This suggests that ghost forces are responsible for the large error. In addition, the quasi-nonlocal QC method yields better approximations to the bifurcation parameters. We also propose arc length parameterization to obtain *quantitative* estimates for the approximation of the bifurcation curves.

The first lattice model for fracture was constructed in [43, 18] to understand the atomic aspect of crack initiation, which led to the important concept of lattice trapping. We have modified the original model so that the QC methods can be directly applied. The modification is necessary because for the spring constant chosen in the original model, the corresponding continuum limit is a fourth order elliptic PDE, rather than a second order one. Despite the modification, the qualitative behavior of the system does not change. In fact, the bifurcation pattern remains the same, and it is still governed by two parameters. The lattice model considered here is a simplified molecular mechanics model, used as a test problem to study multiscale methods. In particular, three methods, including the original QC method, the quasi-nonlocal QC method [40], and a force-based method [21], are considered in this paper. For each method, we derive an effective equation that describes the bifurcation diagram. This is in the same spirit as the center manifold [4], a tool that significantly reduces the dimension of the problem. The one-dimensional lattice model, despite its simplicity, gives rise to bifurcation patterns that resemble those of high-dimensional fracture

Copyright © by SIAM. Unauthorized reproduction of this article is prohibited.

models [23, 24]. Therefore, it already captures the essential mechanism behind crack initiation.

This provides a new approach for measuring the modeling error: Instead of comparing the atomic displacement, which may not have an error bound near bifurcation points, we compare the bifurcation curves. Intuitively, when the bifurcation curves are accurately produced, the transition mechanism is well captured. To quantitatively estimate the error in predicting the bifurcation curves, we formulate the bifurcation equations as solutions of some ODEs. Then, the difference between the bifurcation curves for the full atomistic model and the coupled models can be estimated using the stability theory of ODEs. Since this is a new issue that has not been addressed in previous works, we have chosen the simple lattice model of fracture to illustrate the ideas. For this particular example, we are able to find explicitly the parameters in the bifurcation diagram and make direct comparisons. The extension to more general problems will be investigated in future works.

The rest of the paper has been organized as follows. In section 2, we introduce the lattice model and find the explicit solution of this model. The bifurcation behavior is also discussed. In section 3, we obtain the bifurcation diagrams of three QC approximations. In section 4, we quantify the difference among the bifurcation curves.

2. The lattice fracture model.

2.1. The lattice model. We consider a one-dimensional chain model for crack propagation, which has been used to study the lattice trapping effect [43, 18]. The system consists of two chains of atoms above and below the crack face. Described as "atoms on the rail" [43], the atoms are only allowed to move vertically. The displacement of the atoms is denoted by u_j, $j \geq 0$. This is illustrated in Figure 1.

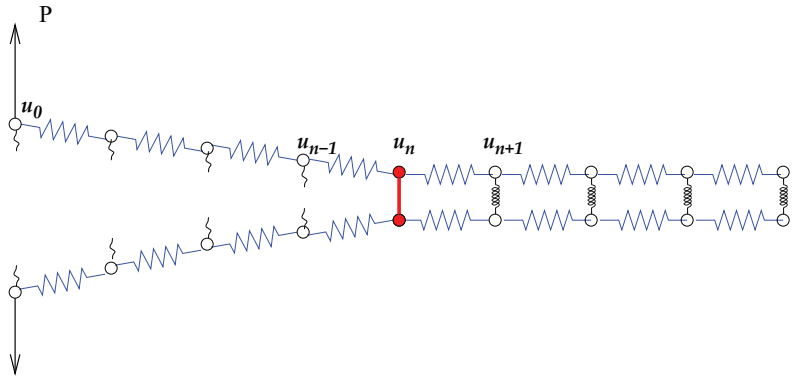

FIG. 1. *A schematic of the lattice model. The springs indicate linear interactions between two atoms. The solid line represents a nonlinear bond at the crack tip.*

Each atom of the chain interacts with the two nearest atoms on the left and the two nearest atoms on the right. In addition, it interacts with the atom below (or above) via a nonlinear force, which is denoted by $F(u)$ and satisfies the following conditions:

1. $\kappa_3 = -F'(0) > 0$.
2. $F(u) = 0$ if $u > u_{\text{cut}}$.
3. $F \in C^1[0, +\infty)$. In particular, we have $F'(u_{\text{cut}}) = 0$.

Copyright © by SIAM. Unauthorized reproduction of this article is prohibited.

Downloaded 02/26/15 to 124.16.148.3. Redistribution subject to SIAM license or copyright; see http://www.siam.org/journals/ojsa.php

Downloaded 02/26/15 to 124.16.148.3. Redistribution subject to SIAM license or copyright; see http://www.siam.org/journals/ojsa.php

Here $u_{\rm cut}$ is a cut-off distance, and bonds are considered to be *broken* beyond this threshold. The first condition states that the nonlinear force, when linearized around the equilibrium position, has spring constant κ_3. The second property is introduced to allow the bond to break when it is severely stretched. The last condition is a smoothness assumption often made in the analysis. The following simple example of $F(u)$ satisfies all those conditions:

$$F(u) = -\frac{\kappa_3}{u_{\rm cut}^2} u(u-u_{\rm cut})^2 \chi_{[0,u_{\rm cut}]}(u), \tag{2.1}$$

where $\chi_{[0,u_{\rm cut}]}$ is a characteristic function.

To mimic a mode-I loading, a force with magnitude P is applied to the zeroth atom as well as the atom below. This serves as a traction condition at the left boundary. We assume that the vertical bonds are already broken for $j < n$ with n the crack-tip position. This creates an existing crack and allows us to study crack propagation. We further simplify the model by replacing the nonlinear bonds ahead of the crack tip by linear springs with spring constant κ_3.

The total potential energy for the upper chain reads as

$$\begin{aligned} E = &-Pu_0 + \sum_{j\geq 0}\Big(\frac{\kappa_1}{2}\big(u_{j+1}-u_j\big)^2 + \frac{\kappa_2}{2}\big(u_{j+2}-u_j\big)^2\Big) \\ &+ n\gamma_0 + \gamma(u_n) + \kappa_3 \sum_{j>n} u_j^2, \end{aligned}$$

where κ_1 and κ_2 are, respectively, the force constants for the nearest and next nearest neighbor interactions. We now explain the various terms in the energy. By assuming that the displacement of the upper chain is exactly the opposite of the displacement of the lower chain, it suffices to count only the energy of the upper atoms. As a result, the energy for each vertical bond ahead of the crack tip is given by $\frac{1}{2}\kappa_3\big[u_j-(-u_j)\big]^2 = 2\kappa_3 u_j^2$. In the total energy, we took half of this energy. The surface energy density is defined by

$$\gamma(u) := -\int_0^u F(v)dv,$$

and we denote $\gamma_0 := \gamma(u_{\rm cut})$.

We assume the force constants satisfy

$$\kappa_1 > 0,\ \bar{\kappa} := \kappa_1 + 4\kappa_2 > 0,\ \kappa_3 = \gamma''(0) > 0. \tag{2.2}$$

We denote the cracked region as A and define

$$L^A u_j := \kappa_1(u_{j+1} - 2u_j + u_{j-1}) + \kappa_2(u_{j+2} - 2u_j + u_{j-2}).$$

Similarly, we denote the uncracked region as B and define $L^B u_j := L^A u_j - 2\kappa_3 u_j$. The force balance equations are given by

$$\kappa_1(u_1 - u_0) + \kappa_2(u_2 - u_0) + P = 0, \tag{2.3}$$

$$\kappa_1(u_2 - 2u_1 + u_0) + \kappa_2(u_3 - u_1) = 0, \tag{2.4}$$

$$L^A u_j = 0, \quad j = 2, \ldots, n-1, \tag{2.5}$$

$$L^A u_n + F(u_n) = 0, \tag{2.6}$$

$$L^B u_j = 0, \quad j \geq n+1. \tag{2.7}$$

Copyright © by SIAM. Unauthorized reproduction of this article is prohibited.

Downloaded 02/26/15 to 124.16.148.3. Redistribution subject to SIAM license or copyright; see http://www.siam.org/journals/ojsa.php

2.2. The solution near the crack tip. In this section, we study the solution at the crack tip by eliminating other degrees of freedom. We start with the atoms along the crack face, where we have a difference equation with the following characteristic equation:

$$p^A(z) = 0, \quad p^A(z) := \kappa_2 z^4 + \kappa_1 z^3 - 2(\kappa_1 + \kappa_2) z^2 + \kappa_1 z + \kappa_2.$$

We factor $p^A(z)$ as $p^A(z) = (z-1)^2(z-z_0)(z-z_0^{-1})$, where

$$z_0 = -1 - \frac{\kappa_1}{2\kappa_2}(1 - \sqrt{\overline{\kappa}/\kappa_1}\,).$$

By (2.2), one can verify that $z_0 < 1$, and z_0 and $1/z_0$ solve

$$\kappa_2 z^2 + (\kappa_1 + 2\kappa_2) z + \kappa_2 = 0. \tag{2.8}$$

Next we turn to the region ahead of the crack tip, where the characteristic equation is

$$p^B(z) = 0 \quad \text{with} \quad p^B(z) := \kappa_2 z^4 + \kappa_1 z^3 - 2(\kappa_1 + \kappa_2 + \kappa_3) z^2 + \kappa_1 z + \kappa_2.$$

In this case, the general solutions can be written as

$$u_j^B = B_1 z_1^j + B_2 z_2^j, \tag{2.9}$$

where z_1 and z_2 are two roots of the characteristic equation that are less than or equal to one. They are selected to ensure that the solution remains bounded as $j \to +\infty$. We focus on the case when all the roots are real. This occurs when $\overline{\kappa}^2 + 8\kappa_2\kappa_3 > 0$. This is not motivated by any physical intuition, but it will simplify the calculations.

Once we have z_1 and z_2, the polynomial $p^B(z)$ can be factored into

$$p^B(z) = \kappa_2 (z - z_1)(z - z_1^{-1})(z - z_2)(z - z_2^{-1}).$$

By comparing the coefficients, we find that

$$\kappa_1 z_1 z_2 = -\kappa_2 (1 + z_1 z_2)(z_1 + z_2). \tag{2.10}$$

This equation will be used later to simplify our calculation.

At the interface, we have the matching conditions:

$$u_i^A = u_i^B, \qquad i = n,\ n-1.$$

For brevity, we drop the superscripts A and B whenever there is no confusion. By setting j to $n-1, n, n+1$, and $n+2$ in (2.9), we find that

$$u_{n+1} = \alpha u_{n-1} + \beta u_n$$

and

$$u_{n+2} = \alpha u_n + \beta u_{n+1} = \alpha\beta u_{n-1} + (\alpha + \beta^2) u_n,$$

where $\alpha = -z_1 z_2,\ \beta = z_1 + z_2$. For other atoms in this region, the displacement can be obtained recursively as

$$u_{j+1} = \alpha u_{j-1} + \beta u_j \quad \text{for any } j \geq n+1.$$

Copyright © by SIAM. Unauthorized reproduction of this article is prohibited.

In terms of the strain, these conditions can be expressed as

$$\begin{aligned} u_{n+1} - u_n &= -\alpha(u_n - u_{n-1}) + (\alpha + \beta - 1)u_n, \\ u_{n+2} - u_n &= -\alpha\beta(u_n - u_{n-1}) + (\alpha\beta + \beta^2 + \alpha - 1)u_n. \end{aligned} \tag{2.11}$$

By (2.10), we find that

$$\kappa_1\alpha + \kappa_2(\alpha - 1)\beta = 0, \quad 2(\kappa_1 + \kappa_2)\alpha + \kappa_2(\alpha^2 + \beta^2 + 1) = 2\kappa_3\alpha. \tag{2.12}$$

With these preparations, we are ready to find solutions in the crack region. For $j \le n + 1$, we express the solution as

$$u_j = a + bj + c\cosh[j\delta] + d\sinh[j\delta] \tag{2.13}$$

with

$$\cosh\delta = -1 - \kappa_1/(2\kappa_2). \tag{2.14}$$

In particular, we choose $\delta = -\log z_0$.

We proceed to derive an equation for u_n by eliminating all other variables in $L^A u_n$. It follows from (2.11) that

$$\begin{aligned} L^A u_n &= \kappa_2(u_{n+2} - u_n) + \kappa_1(u_{n+1} - u_n) \\ &\quad - (\kappa_1 + \kappa_2)(u_n - u_{n-1}) - \kappa_2(u_{n-1} - u_{n-2}) \\ &= \big[\kappa_1(\alpha + \beta - 1) + \kappa_2(\alpha\beta + \beta^2 + \alpha - 1)\big]u_n \\ &\quad - \big[\kappa_1(1 + \alpha) + \kappa_2(1 + \alpha\beta)\big](u_n - u_{n-1}) - \kappa_2(u_{n-1} - u_{n-2}) \\ &= (\alpha + \beta - 1)\big(\kappa_1 + \kappa_2(1 + \beta)\big)u_n \\ &\quad - \big(\big(\kappa_1 + \kappa_2(1 + \beta)\big)(u_n - u_{n-1}) + \kappa_2(u_{n-1} - u_{n-2})\big), \end{aligned} \tag{2.15}$$

where we have used the identity

$$\kappa_1(1 + \alpha) + \kappa_2(1 + \alpha\beta) = \kappa_1 + \kappa_2(1 + \beta),$$

which follows from (2.12). To calculate the second term in (2.15), we use the following relations that can be easily verified, and the proof can be found in Appendix A.

For any $k \in \mathbb{Z}$, there holds that

$$\begin{aligned} &(\kappa_1 + 2\kappa_2)(\cosh[k\delta] - \cosh[(k-1)\delta]) + \kappa_2(\cosh[(k-1)\delta] - \cosh[(k-2)\delta]) \\ &\qquad = -\kappa_2(\cosh[(k+1)\delta] - \cosh[k\delta]) \end{aligned} \tag{2.16}$$

and

$$\begin{aligned} &(\kappa_1 + 2\kappa_2)(\sinh[k\delta] - \sinh[(k-1)\delta]) + \kappa_2(\sinh[(k-1)\delta] - \sinh[(k-2)\delta]) \\ &\qquad = -\kappa_2(\sinh[(k+1)\delta] - \sinh[k\delta]). \end{aligned} \tag{2.17}$$

For any $k \in \mathbb{Z}$ and $\rho \in \mathbb{R}$, we define

$$\begin{aligned} \mathcal{F}_{k,\rho}(\delta) &:= \cosh[(k+1)\delta] - (1-\rho)\cosh[k\delta] - \rho\cosh[(k-1)\delta], \\ \mathcal{G}_{k,\rho}(\delta) &:= \sinh[(k+1)\delta] - (1-\rho)\sinh[k\delta] - \rho\sinh[(k-1)\delta]. \end{aligned}$$

Copyright © by SIAM. Unauthorized reproduction of this article is prohibited.

Downloaded 02/26/15 to 124.16.148.3. Redistribution subject to SIAM license or copyright; see http://www.siam.org/journals/ojsa.php

Downloaded 02/26/15 to 124.16.148.3. Redistribution subject to SIAM license or copyright; see http://www.siam.org/journals/ojsa.php

Using (2.16) and (2.17) with $k = n$ and $\rho = 1 - \beta$, we obtain

$$\begin{aligned}\big(\kappa_1 + \kappa_2(\beta+1)\big)(u_n - u_{n-1}) + \kappa_2(u_{n-1} - u_{n-2}) \\ = \big(\overline{\kappa} + \kappa_2(\beta-2)\big)b - \kappa_2\big(\mathcal{F}_{n,1-\beta}(\delta)c + \mathcal{G}_{n,1-\beta}(\delta)d\big).\end{aligned}$$

Substituting the above identity into (2.15), we obtain

$$\begin{aligned}L^A u_n = (\alpha+\beta-1)\big(\kappa_1 + \kappa_2(1+\beta)\big)u_n \\ - \big(\overline{\kappa} + \kappa_2(\beta-2)\big)b + \kappa_2\big(\mathcal{F}_{n,1-\beta}(\delta)c + \mathcal{G}_{n,1-\beta}(\delta)d\big).\end{aligned} \tag{2.18}$$

It remains to find the parameters b, c, and d. First we substitute the expressions for $u_{n+1} - u_n$ and $u_n - u_{n-1}$ into (2.11) and obtain

$$\mathcal{F}_{n,\alpha}(\delta)c + \mathcal{G}_{n,\alpha}(\delta)d = -(1+\alpha)b + (\alpha+\beta-1)u_n. \tag{2.19}$$

Next we shall use the equations for $j = 1, 2$ to determine two parameters in u_j. A simple trick is to introduce one more atom to the left, with displacement, $u_{\bar{1}}$, and extend the equation to $j = 1$,

$$\kappa_1(u_2 - 2u_1 + u_0) + \kappa_2(u_3 - 2u_1 + u_{\bar{1}}) = 0,$$

which together with (2.4) leads to $u_1 = u_{\bar{1}}$. This immediately implies

$$b = -d\sinh\delta.$$

Substituting the expression of u_j into (2.3), we obtain

$$(\cosh\delta - 1)\left(\kappa_1 + 2\kappa_2(\cosh\delta + 1)\right)c + 2\kappa_2\sinh\delta(\cosh\delta - 1)d + P = 0.$$

Using (2.14), we obtain

$$d = -\frac{P}{2\kappa_2\sinh\delta(\cosh\delta - 1)} = \frac{P/\overline{\kappa}}{\sinh\delta},$$

which in turn implies $b = -P/\overline{\kappa}$. Finally, we solve (2.19)[1] with the above expressions for b and d and obtain

$$c = \frac{\alpha+\beta-1}{\mathcal{F}_{n,\alpha}(\delta)}u_n - \frac{P/\bar{\kappa}}{\mathcal{F}_{n,\alpha}(\delta)}\left(\frac{\mathcal{G}_{n,\alpha}(\delta)}{\sinh\delta} - (1+\alpha)\right).$$

Substituting the expressions of b, c, and d into (2.18), we obtain an equation for u_n:

$$F(u_n) + \kappa u_n + \eta P = 0 \tag{2.20}$$

with

$$\kappa = (\alpha+\beta-1)\left(\kappa_1 + \kappa_2(1+\beta) + \kappa_2\frac{\mathcal{F}_{n,1-\beta}(\delta)}{\mathcal{F}_{n,\alpha}(\delta)}\right)$$

and

$$\eta = \frac{\kappa_2}{\overline{\kappa}}\left(\frac{\mathcal{G}_{n,1-\beta}\mathcal{F}_{n,\alpha} - \mathcal{F}_{n,1-\beta}\mathcal{G}_{n,\alpha}}{\sinh\delta\mathcal{F}_{n,\alpha}} + (1+\alpha)\frac{\mathcal{F}_{n,1-\beta}}{\mathcal{F}_{n,\alpha}}\right) + \frac{\kappa_1 + \kappa_2(1+\beta)}{\overline{\kappa}}.$$

[1]This relation is possible because we have assumed that only the roots with magnitude less than one in the expression of u_j.

Copyright © by SIAM. Unauthorized reproduction of this article is prohibited.

Downloaded 02/26/15 to 124.16.148.3. Redistribution subject to SIAM license or copyright; see http://www.siam.org/journals/ojsa.php

Equation (2.20) is called *the effective equation* because all other degrees of freedom have been removed. Of particular interest are the limits of κ and η when n is large. To this end, we write

$$\big(\mathcal{F}_{n,\alpha}(\delta), \mathcal{G}_{n,\alpha}(\delta)\big) = \big(A_\alpha(\delta), B_\alpha(\delta)\big)\mathcal{K}_n$$

with $A_\alpha(\delta) = (1-\alpha)(\cosh\delta - 1)$ and $B_\alpha(\delta) = (1+\alpha)\sinh\delta$, and the 2 by 2 matrix $\mathcal{K}_n$ is defined by

$$\mathcal{K}_n := \begin{pmatrix} \cosh[n\delta] & \sinh[n\delta] \\ \sinh[n\delta] & \cosh[n\delta] \end{pmatrix}.$$

A direct calculation gives $\kappa \to \kappa_0$ as $n \to \infty$ with

$$\kappa_0 = (\alpha+\beta-1)\left(\kappa_1 + \kappa_2(1+\beta) + \kappa_2 \frac{A_{1-\beta}(\delta) + B_{1-\beta}(\delta)}{A_\alpha(\delta) + B_\alpha(\delta)}\right).$$

This is the limit when the length of the crack reaches a macroscopic size. In particular, we have an expansion of κ as

$$\kappa = \kappa_0 - \frac{(\alpha+\beta-1)\overline{\kappa}\sinh\delta}{(A_\alpha(\delta)+B_\alpha(\delta))^2} z_0^{2n} + \mathcal{O}(z_0^{4n}).$$

To calculate the limit of η, we write

$$\begin{aligned} \mathcal{G}_{n,1-\beta}\mathcal{F}_{n,\alpha} - \mathcal{F}_{n,1-\beta}\mathcal{G}_{n,\alpha} &= \det\begin{pmatrix} \mathcal{F}_{n,\alpha} & \mathcal{F}_{n,1-\beta} \\ \mathcal{G}_{n,\alpha} & \mathcal{G}_{n,1-\beta} \end{pmatrix} = \det\mathcal{K}_n \det\begin{pmatrix} A_\alpha & A_{1-\beta} \\ B_\alpha & B_{1-\beta} \end{pmatrix} \\ &= -2(\alpha+\beta-1)(\cosh\delta-1)\sinh\delta. \end{aligned} \tag{2.21}$$

Substituting the above identity into the expression of η, we obtain

$$\eta = 1 + \frac{\kappa_2}{\overline{\kappa}} \frac{(\beta-2)\mathcal{F}_{n,\alpha} + (1+\alpha)\mathcal{F}_{n,1-\beta}}{\mathcal{F}_{n,\alpha}} - \frac{2\kappa_2}{\overline{\kappa}} \frac{(\alpha+\beta-1)(\cosh\delta-1)}{\mathcal{F}_{n,\alpha}}.$$

A direct calculation gives

$$\begin{aligned} (\beta-2)\mathcal{F}_{n,\alpha} + (1+\alpha)\mathcal{F}_{n,1-\beta} &= ((\beta-2)A_\alpha + (1+\alpha)A_{1-\beta})\cosh[n\delta] \\ &= 2(\alpha+\beta-1)(\cosh\delta-1)\cosh[n\delta]. \end{aligned} \tag{2.22}$$

Using the above identity, we rewrite η as

$$\begin{aligned} \eta &= 1 + \frac{2\kappa_2}{\overline{\kappa}} \frac{(\alpha+\beta-1)(\cosh\delta-1)(\cosh[n\delta]-1)}{\mathcal{F}_{n,\alpha}} \\ &= 1 - \frac{(\alpha+\beta-1)(\cosh[n\delta]-1)}{\mathcal{F}_{n,\alpha}}. \end{aligned} \tag{2.23}$$

Letting n go to infinity, we obtain $\eta \to \eta_0$ with

$$\eta_0 = 1 - \frac{\alpha+\beta-1}{A_\alpha(\delta)+B_\alpha(\delta)}.$$

We also have the following expansion for η:

$$\eta = \eta_0 + \frac{2(\alpha+\beta-1)}{A_\alpha(\delta)+B_\alpha(\delta)} z_0^n + \mathcal{O}(z_0^{2n}).$$

Notice that we have $\kappa_0 < 0$, since

$$\alpha+\beta-1 = -(1-z_1)(1-z_2) < 0, \tag{2.24}$$

and similarly, we have $\eta_0 > 1$.

Copyright © by SIAM. Unauthorized reproduction of this article is prohibited.

2.3. Bifurcation behavior. To understand the roles of the parameters κ and η, we rewrite the reduced equation (2.20) as

$$\kappa u + \eta P = -F(u). \tag{2.25}$$

We shall regard κ as an intrinsic material parameter and P as an external load that can be varied. Various cases can be directly observed from Figure 2 by comparing the linear function on the left-hand side and $-F(u)$ on the right-hand side. For two particular values of P, the linear function becomes tangent to $-F(u)$. They correspond to two bifurcation points of saddle-node type. In spite of the simplicity of the one-dimensional lattice model, the bifurcation seems to be quite generic. In fact, the same type of bifurcations have been observed in two- and three-dimensional lattice models [23], where a sequence of saddle-node bifurcations was observed.

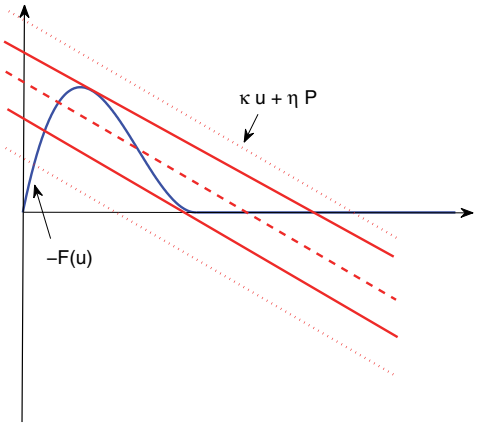

FIG. 2. *The solutions of* (2.20)*, shown as the intersections of the function* $-F(u)$ *and the linear function* $\kappa u + \eta P$*. Dotted lines: Only one solution exists. The dashed line: There are three solutions. Solid lines: Two of the three solutions reduce to a repeated root.*

In what follows, we will turn to the QC approximation models and investigate how the bifurcation diagram is influenced by the QC approximation.

3. Crack-tip solutions and bifurcation curves for the multiscale models. We analyze three QC methods applied to the above lattice model. The calculation will be carried out as explicitly as possible, with the goal of not overestimating the error. Due to the discrete nature of the model, the calculation is quite lengthy. We will only show the full details for the first model and keep the procedure brief for the other two models.

3.1. The quasi-continuum method without force correction. The original QC method [42] relies on an energy summation rule. In the cracked region, the total energy can be written as a sum of the site energy, i.e., $E = \sum_j V_j$ with

$$V_j = \frac{\kappa_1}{4}\left((u_{j+1}-u_j)^2 + (u_{j-1}-u_j)^2\right) + \frac{\kappa_2}{4}\left((u_{j+2}-u_j)^2 + (u_{j-2}-u_j)^2\right).$$

Moreover, for the atoms at and behind the crack tip, an energy functional for the vertical bonds should be included in the total energy.

Copyright © by SIAM. Unauthorized reproduction of this article is prohibited.

Downloaded 02/26/15 to 124.16.148.3. Redistribution subject to SIAM license or copyright; see http://www.siam.org/journals/ojsa.php

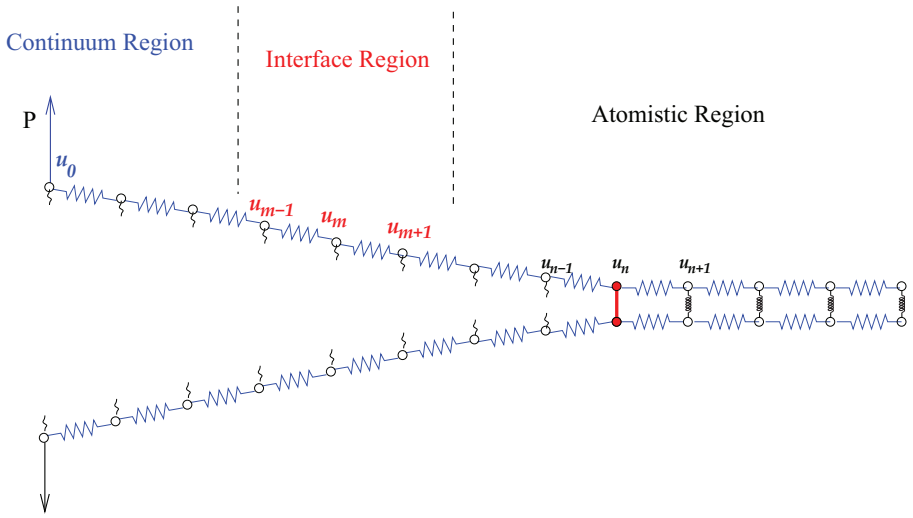

FIG. 3. *A schematic illustration of the QC method applied to the lattice model. The local region (continuum) includes the atoms $j < m$, and the nonlocal region (atomistic) is defined to contain atoms $j > m$. Due to the second nearest neighbor interaction, the interface region involves three atoms.*

The QC method introduces a *local* region, where the displacement field is represented on a finite element mesh, and within each element, the energy is approximated by the Cauchy–Born (CB) rule [3]. To separate out the issue of interpolation and quadrature error, we assume that the mesh node coincides with the atom position. In this case, the approximating energy takes the form of $E_{\mathrm{QC}} = \sum_i E_i$, where the summation is over all the atom sites. We assume that the local region includes atoms $j < m-1$, as indicated in Figure 3, and the approximating energy is given by

$$E_j = \frac{\overline{\kappa}}{2}\left[(u_{j+1}-u_j)^2 + (u_j - u_{j-1})^2\right] \qquad \text{for} \quad j < m-1$$

as a result of the CB approximation. In addition, we have

$$E_j = V_j \qquad \text{for} \quad m < j < n.$$

At the interface, the energy functions are given by

$$\begin{aligned} E_{m-1} &= \frac{\kappa_1}{4}\left((u_m - u_{m-1})^2 + (u_{m-1}-u_{m-2})^2\right) \\ &\quad + \kappa_2\left((u_m - u_{m-1})^2 + (u_{m-1}-u_{m-2})^2\right), \\ E_m &= \frac{\kappa_1}{4}\left((u_m - u_{m-1})^2 + (u_{m+1}-u_m)^2\right) \\ &\quad + \frac{\kappa_2}{4}\left((u_{m+2} - u_m)^2 + 4(u_m - u_{m-1})^2\right). \end{aligned}$$

We have the following system of equilibrium equations:

$$\begin{cases} \overline{\kappa}(u_1 - u_0) + P = 0, & \\ \overline{\kappa}(u_{j+1} - 2u_j + u_{j-1}) = 0, & 2 \le j \le m-2, \\ L^A u_j = 0, & m-1 \le j \le n-1, \\ L^A u_n + F(u_n) = 0, & \\ L^B u_j = 0, & j \ge n+1. \end{cases} \tag{3.1}$$

Copyright © by SIAM. Unauthorized reproduction of this article is prohibited.

Downloaded 02/26/15 to 124.16.148.3. Redistribution subject to SIAM license or copyright; see http://www.siam.org/journals/ojsa.php

Downloaded 02/26/15 to 124.16.148.3. Redistribution subject to SIAM license or copyright; see http://www.siam.org/journals/ojsa.php

Around the interface, we have the following coupling equations:

$$\begin{cases} \overline{\kappa}u_{m-2} - (2\kappa_1 + 17\kappa_2/2)\, u_{m-1} + \overline{\kappa}u_m + \dfrac{\kappa_2}{2}u_{m+1} = 0, \\ \overline{\kappa}u_{m-1} - (2\kappa_1 + 5\kappa_2)u_m + \kappa_1 u_{m+1} + \kappa_2 u_{m+2} = 0, \\ \dfrac{\kappa_2}{2}u_{m-1} + \kappa_1 u_m - (2\kappa_1 + 3\kappa_2/2)\, u_{m+1} + \kappa_1 u_{m+2} + \kappa_2 u_{m+3} = 0. \end{cases} \tag{3.2}$$

In practice, the atomistic region should be defined around the crack tip in a multiscale coupling method. Because the calculations in this paper are already quite involved, we introduced only the continuum region to the left of the crack tip.

To proceed, we notice that in the local region,

$$u_j = C_0 + C_1 j, \quad j = 0, 1, \ldots, m-1,$$

for certain constants C_0 and C_1. If we impose the traction boundary condition, then the solution takes a simpler form as

$$u_j = C_0 + \frac{P}{\overline{\kappa}}(m - j - 1). \tag{3.3}$$

Adding up all the equations in (3.2), we obtain

$$(\kappa_1 + \kappa_2)(u_{m+2} - u_{m+1}) + \kappa_2(u_{m+3} - u_m) = -\overline{\kappa}(u_{m-2} - u_{m-1}) = -P,$$

where we have used (3.3) in the last step.

We substitute (3.3) into the first two equations of (3.2) and obtain

$$\begin{aligned} (\kappa_1 + 9\kappa_2/2)(u_m - u_{m-1}) - \frac{\kappa_2}{2}(u_{m+1} - u_m) &= -P, \\ -\overline{\kappa}(u_m - u_{m-1}) + \kappa_1(u_{m+1} - u_m) + \kappa_2(u_{m+2} - u_m) &= 0. \end{aligned}$$

Denote $\gamma = \overline{\kappa}/[\overline{\kappa} + \kappa_2/2]$. We eliminate $u_m - u_{m-1}$ from the above two equations and obtain the following linear system:

$$\begin{cases} \left[\kappa_1 + \dfrac{\gamma}{2}\kappa_2\right](u_{m+1} - u_m) + \kappa_2(u_{m+2} - u_m) = -\gamma P, \\ (\kappa_1 + \kappa_2)(u_{m+2} - u_{m+1}) + \kappa_2(u_{m+3} - u_{m+1}) = -P. \end{cases} \tag{3.4}$$

To proceed, we express the solution in the atomistic region before the crack tip in the same form as in the previous section for $j = m-3, \ldots, n+1$:

$$u_j = a + bj + c\cosh[j\delta] + d\sinh[j\delta]. \tag{3.5}$$

We substitute the above ansatz into (3.4) and obtain

$$(c, d)\mathcal{K}_m = (P, b)\mathcal{Q}, \tag{3.6}$$

where $\mathcal{Q} = \{q_{ij}\}_{i,j=1}^2$ is a 2 by 2 matrix given by

$$\mathcal{Q} := \frac{1}{4\kappa_2}\begin{pmatrix} \dfrac{4 - 3\gamma}{\cosh\delta - 1} & \dfrac{3\gamma}{\sinh\delta} \\ \dfrac{(2-\gamma)\overline{\kappa}}{\cosh\delta - 1} & \dfrac{(\gamma+2)\overline{\kappa} - 4\kappa_2}{\sinh\delta} \end{pmatrix}.$$

Copyright © by SIAM. Unauthorized reproduction of this article is prohibited.

The details are postponed to Appendix A.

Using the fact that $\mathcal{K}_m^{-1}\mathcal{K}_n = \mathcal{K}_{n-m}$, we get

$$\begin{aligned}\mathcal{F}_{n,\alpha}(\delta)c + \mathcal{G}_{n,\alpha}(\delta)d &= (c,d)\mathcal{K}_n(A_\alpha, B_\alpha)^T = (P,b)\mathcal{Q}\mathcal{K}_m^{-1}\mathcal{K}_n(A_\alpha, B_\alpha)^T \\ &= (P,b)\mathcal{Q}\mathcal{K}_{n-m}(A_\alpha, B_\alpha)^T = (P,b)\mathcal{Q}\left(\mathcal{F}_{n-m,\alpha}, \mathcal{G}_{n-m,\alpha}\right)^T.\end{aligned}$$

Using (2.19), we represent b in terms of u_n and P as

$$b = \frac{\alpha+\beta-1}{q_{21}\mathcal{F}_{n-m,\alpha} + q_{22}\mathcal{G}_{n-m,\alpha} + 1 + \alpha}u_n - \frac{q_{11}\mathcal{F}_{n-m,\alpha} + q_{12}\mathcal{G}_{n-m,\alpha}}{q_{21}\mathcal{F}_{n-m,\alpha} + q_{22}\mathcal{G}_{n-m,\alpha} + 1 + \alpha}P.$$

A direct calculation gives

$$\begin{aligned}\mathcal{F}_{n,1-\beta}(\delta)c + \mathcal{G}_{n,1-\beta}(\delta)d = &\left(q_{21}\mathcal{F}_{n-m,1-\beta} + q_{22}\mathcal{G}_{n-m,1-\beta}\right)b \\ &+ \left(q_{11}\mathcal{F}_{n-m,1-\beta} + q_{12}\mathcal{G}_{n-m,1-\beta}\right)P.\end{aligned}$$

Now we find the effective equation for u_n:

$$F(u) + \kappa^{\mathrm{qc}}u + \eta^{\mathrm{qc}}P = 0$$

with

$$\begin{aligned}\kappa^{\mathrm{qc}} = &(\alpha+\beta-1)\left(\kappa_1 + \kappa_2(1+\beta) + \kappa_2\frac{q_{21}\mathcal{F}_{n-m,1-\beta} + q_{22}\mathcal{G}_{n-m,1-\beta}}{q_{21}\mathcal{F}_{n-m,\alpha} + q_{22}\mathcal{G}_{n-m,\alpha} + 1 + \alpha}\right) \\ &- (\alpha+\beta-1)\frac{\overline{\kappa} + (\beta-2)\kappa_2}{q_{21}\mathcal{F}_{n-m,\alpha} + q_{22}\mathcal{G}_{n-m,\alpha} + 1 + \alpha}\end{aligned}$$

and

$$\begin{aligned}\eta^{\mathrm{qc}} = &\kappa_2\left(q_{11}\mathcal{F}_{n-m,1-\beta} + q_{12}\mathcal{G}_{n-m,1-\beta}\right) \\ &- \kappa_2\frac{\left(q_{11}\mathcal{F}_{n-m,\alpha} + q_{12}\mathcal{G}_{n-m,\alpha}\right)\left(q_{21}\mathcal{F}_{n-m,1-\beta} + q_{22}\mathcal{G}_{n-m,1-\beta}\right)}{q_{21}\mathcal{F}_{n-m,\alpha} + q_{22}\mathcal{G}_{n-m,\alpha} + 1 + \alpha} \\ &+ \frac{\left(q_{11}\mathcal{F}_{n-m,\alpha} + q_{12}\mathcal{G}_{n-m,\alpha}\right)\left(\overline{\kappa} + (\beta-2)\kappa_2\right)}{q_{21}\mathcal{F}_{n-m,\alpha} + q_{22}\mathcal{G}_{n-m,\alpha} + 1 + \alpha}.\end{aligned}$$

Letting $n-m \to \infty$, we obtain $\kappa^{\mathrm{qc}} \to \kappa_0$ with the expansion

$$\kappa^{\mathrm{qc}} = \kappa_0 + \frac{2(\alpha+\beta-1)(\alpha+\beta-1-A_\alpha-B_\alpha)\overline{\kappa}}{(q_{21}+q_{22})(A_\alpha(\delta)+B_\alpha(\delta))^2}z_0^{n-m} + \mathcal{O}(z_0^{2(n-m)}).$$

Proceeding along the same line that leads to (2.21), we obtain

$$\begin{aligned}&\left(q_{11}\mathcal{F}_{n-m,1-\beta} + q_{12}\mathcal{G}_{n-m,1-\beta}\right)\left(q_{21}\mathcal{F}_{n-m,\alpha} + q_{22}\mathcal{G}_{n-m,\alpha}\right) \\ &\quad - \left(q_{11}\mathcal{F}_{n-m,\alpha} + q_{12}\mathcal{G}_{n-m,\alpha}\right)\left(q_{21}\mathcal{F}_{n-m,1-\beta} + q_{22}\mathcal{G}_{n-m,1-\beta}\right) \\ &= \det\left[\begin{pmatrix}\mathcal{F}_{n-m,1-\beta} & \mathcal{G}_{n-m,1-\beta}\\ \mathcal{F}_{n-m,\alpha} & \mathcal{G}_{n-m,\alpha}\end{pmatrix}\mathcal{Q}\right] = \det\left[\begin{pmatrix}A_{1-\beta} & B_{1-\beta}\\ A_\alpha & B_\alpha\end{pmatrix}\mathcal{K}_{n-m}\mathcal{Q}\right] \\ &= -(\alpha+\beta-1)\left(2(1-\gamma)\overline{\kappa} - (4-3\gamma)\kappa_2\right)/(2\kappa_2^2).\end{aligned}$$

Using the above identity, we write η^{qc} as

$$\begin{aligned}\eta^{\mathrm{qc}} = &\frac{q_{11}\mathcal{F}_{n-m,\alpha} + q_{12}\mathcal{G}_{n-m,\alpha}}{q_{21}\mathcal{F}_{n-m,\alpha} + q_{22}\mathcal{G}_{n-m,\alpha} + 1 + \alpha}\left(\overline{\kappa} + (\beta-2)\kappa_2\right) \\ &+ \frac{q_{11}\mathcal{F}_{n-m,1-\beta} + q_{12}\mathcal{G}_{n-m,1-\beta}}{q_{21}\mathcal{F}_{n-m,\alpha} + q_{22}\mathcal{G}_{n-m,\alpha} + 1 + \alpha}(1+\alpha)\kappa_2 \\ &- \frac{(\alpha+\beta-1)\left(2(1-\gamma)\overline{\kappa} - (4-3\gamma)\kappa_2\right)}{2\left(q_{21}\mathcal{F}_{n-m,\alpha} + q_{22}\mathcal{G}_{n-m,\alpha} + 1 + \alpha\right)\kappa_2}.\end{aligned}$$

Copyright © by SIAM. Unauthorized reproduction of this article is prohibited.

Downloaded 02/26/15 to 124.16.148.3. Redistribution subject to SIAM license or copyright; see http://www.siam.org/journals/ojsa.php

Downloaded 02/26/15 to 124.16.148.3. Redistribution subject to SIAM license or copyright; see http://www.siam.org/journals/ojsa.php

By (2.22) and (2.14), we get

$$\begin{aligned}((\beta-2)\mathcal{F}_{n-m,\alpha}+(1+\alpha)\mathcal{F}_{n-m,1-\beta})\,\kappa_2 &= 2(\alpha+\beta-1)\kappa_2(\cosh\delta-1)\cosh[(n-m)\delta]\\ &= (\alpha+\beta-1)\overline{\kappa}\cosh[(n-m)\delta].\end{aligned}$$

Similarly,

$$((\beta-2)\mathcal{G}_{n-m,\alpha}+(1+\alpha)\mathcal{G}_{n-m,1-\beta})\,\kappa_2 = (\alpha+\beta-1)\overline{\kappa}\sinh[(n-m)\delta].$$

Using the above two equations, we rewrite $\eta^{\rm qc}$ as

$$\begin{aligned}\eta^{\rm qc} = {}& \frac{q_{11}\mathcal{F}_{n-m,\alpha}+q_{12}\mathcal{G}_{n-m,\alpha}}{q_{21}\mathcal{F}_{n-m,\alpha}+q_{22}\mathcal{G}_{n-m,\alpha}+1+\alpha}\overline{\kappa}\\ &-(\alpha+\beta-1)\frac{q_{11}\cosh[(n-m)\delta]+q_{12}\sinh[(n-m)\delta]}{q_{21}\mathcal{F}_{n-m,\alpha}+q_{22}\mathcal{G}_{n-m,\alpha}+1+\alpha}\overline{\kappa}\\ &-\frac{(\alpha+\beta-1)[(1-\gamma)\overline{\kappa}/\kappa_2-(2-3\gamma/2)]}{q_{21}\mathcal{F}_{n-m,\alpha}+q_{22}\mathcal{G}_{n-m,\alpha}+1+\alpha}.\end{aligned}$$

Letting $n-m\to\infty$, we obtain $\eta^{\rm qc}\to\eta_0^{\rm qc}$ with

$$\eta_0^{\rm qc} = \left(1-\frac{\alpha+\beta-1}{A_\alpha(\delta)+B_\alpha(\delta)}\right)\frac{q_{11}+q_{12}}{q_{21}+q_{22}}\overline{\kappa} = \frac{q_{11}+q_{12}}{q_{21}+q_{22}}\overline{\kappa}\,\eta_0.$$

A direct calculation gives

$$\eta_0-\eta_0^{\rm qc} = \frac{4+3\gamma(\coth[\delta/2]-1)}{2-\gamma+(\gamma+2-4\kappa_2/\overline{\kappa})\coth[\delta/2]}\eta_0.$$

It is clear that $\eta_0^{\rm qc}$ does not coincide with η_0 as $n-m\to\infty$.

As an example of comparison, we plot the bifurcation diagram for both models in Figure 4. We chose $\kappa_1=4$, $\kappa_2=0.4$, $\kappa_3=20$, and $u_{\rm cut}=0.5$. Clearly, the diagram consists of two saddle-node bifurcation points. Although QC predicts a similar bifurcation behavior, the difference between the bifurcation curves is significant.

3.2. The quasi-nonlocal quasi-continuum method. The quasi-nonlocal quasi-continuum (QQC) method [40] approximates the energy as follows. For $j<m-1$, the site energy is

$$E_j = \frac{\overline{\kappa}}{2}\big((u_{j+1}-u_j)^2+(u_j-u_{j-1})^2\big),$$

and for $j>m$, we set $E_j=V_j$, and at the interface, i.e., for $j=m-1,m$,

$$E_j = \frac{\kappa_2}{4}(u_{j+2}-u_j)^2+\frac{\kappa_1}{4}\big((u_{j+1}-u_j)^2+(u_j-u_{j-1})^2\big)+\kappa_2(u_j-u_{j-1})^2.$$

The resulting force balance equations are the same as those of the original QC (3.1) except the interfacial equations:

$$\begin{cases}\overline{\kappa}(u_{m-2}-u_{m-1})+(\kappa_1+2\kappa_2)(u_m-u_{m-1})+\kappa_2(u_{m+1}-u_{m-1})=0,\\ (\kappa_1+2\kappa_2)(u_{m-1}-u_m)+\kappa_1(u_{m+1}-u_m)+\kappa_2(u_{m+2}-u_m)=0.\end{cases}\tag{3.7}$$

Using a similar procedure that leads to (3.4), we eliminate $u_{m-1}-u_{m-2}$ from (3.7) and obtain

$$\begin{cases}(\kappa_1+2\kappa_2)(u_m-u_{m-1})+\kappa_2(u_{m+1}-u_{m-1})=-P,\\ -(\kappa_1+2\kappa_2)(u_m-u_{m-1})+\kappa_1(u_{m+1}-u_m)+\kappa_2(u_{m+2}-u_m)=0.\end{cases}\tag{3.8}$$

Copyright © by SIAM. Unauthorized reproduction of this article is prohibited.

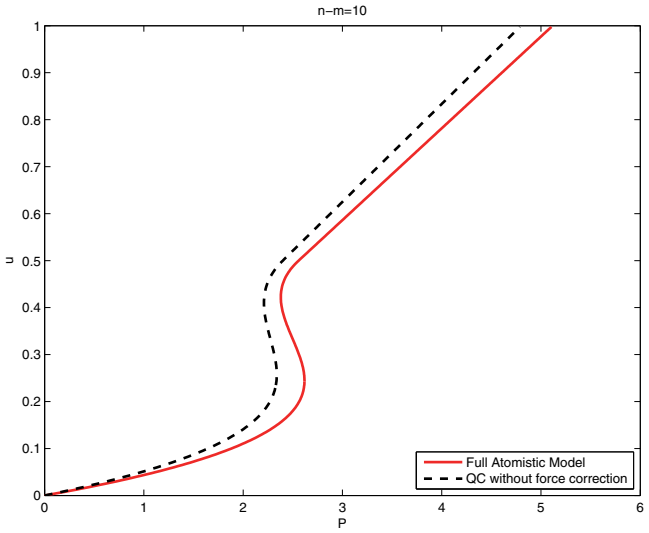

FIG. 4. *The bifurcation diagrams for the full atomistic model and QC without force corrections. The middle branch contains an unstable equilibrium, while the other two branches are stable.*

Substituting the general expression of u_j into the above two equations, we obtain

$$\cosh[(m-1)\delta]\, c + \sinh[(m-1)\delta]\, d = \frac{P}{\overline{\kappa}} + b = 0. \tag{3.9}$$

We leave the details for deriving the above equation to Appendix B. An immediate consequence of the above equation is $b = -P/\overline{\kappa}$, which together with (2.19) yields

$$\mathcal{F}_{n,\alpha}(\delta)c + \mathcal{G}_{n,\alpha}(\delta)d = (\alpha+\beta-1)u_n + (1+\alpha)P/\bar{\kappa}.$$

This equation, together with (3.9), gives

$$\begin{cases} c = -\dfrac{\sinh[(m-1)\delta]}{\mathcal{G}_{n-m+1,\alpha}(\delta)}\big((\alpha+\beta-1)u_n + (1+\alpha)P/\bar{\kappa}\big), \\ d = \dfrac{\cosh[(m-1)\delta]}{\mathcal{G}_{n-m+1,\alpha}(\delta)}\big((\alpha+\beta-1)u_n + (1+\alpha)P/\bar{\kappa}\big). \end{cases}$$

Substituting the expressions of c and d into (2.19), we obtain

$$F(u_n) + \kappa^{\mathrm{qqc}} u_n + \eta^{\mathrm{qqc}} P = 0$$

with

$$\kappa^{\mathrm{qqc}} = (\alpha+\beta-1)\left(\kappa_1 + \kappa_2(1+\beta) + \kappa_2 \frac{\mathcal{G}_{n-m+1,1-\beta}(\delta)}{\mathcal{G}_{n-m+1,\alpha}(\delta)}\right),$$

$$\eta^{\mathrm{qqc}} = 1 - (\alpha+\beta-1)\frac{\sinh[(n-m+1)\delta]}{\mathcal{G}_{n-m+1,\alpha}(\delta)}.$$

We expand these two parameters and get

$$\kappa^{\mathrm{qqc}} = \kappa_0 - \frac{2\overline{\kappa}(\alpha+\beta-1)\sinh\delta}{(A_\alpha+B_\alpha)^2} z_0^{2n-2m+2} + \mathcal{O}(z_0^{4n-4m+4}),$$

$$\eta^{\mathrm{qqc}} = \eta_0 + \frac{2(\alpha+\beta-1)A_\alpha}{(A_\alpha+B_\alpha)^2} z_0^{2n-2m+2} + \mathcal{O}(z_0^{4n-4m+4}).$$

Copyright © by SIAM. Unauthorized reproduction of this article is prohibited.

Downloaded 02/26/15 to 124.16.148.3. Redistribution subject to SIAM license or copyright; see http://www.siam.org/journals/ojsa.php

Letting $n - m \to \infty$, we obtain $\kappa \to \kappa_0$ and $\eta \to \eta_0$. The limits κ_0 and η_0 are the same as those of the atomistic model. Namely, QQC gives the correct bifurcation diagram in the limit, which is confirmed by a comparison of the bifurcation diagram, as illustrated in Figure 5, where excellent agreement is observed. In fact the bifurcation curve is indistinguishable from the exact one. To reach this asymptotic regime, the crack tip has to be sufficiently far away from the atomistic/continuum interface.

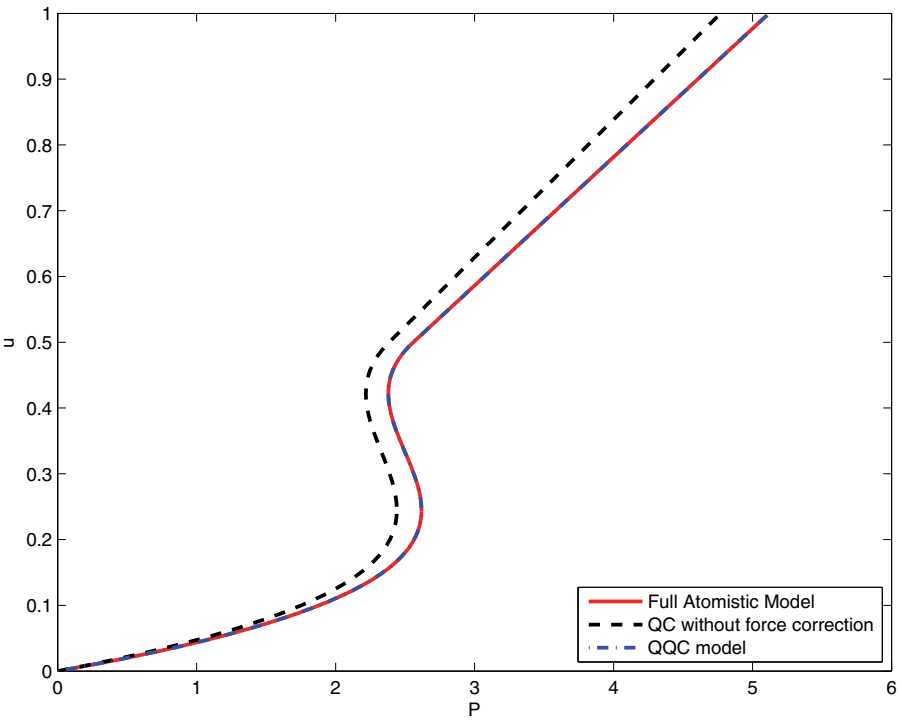

FIG. 5. *The bifurcation diagrams for the QC and QQC methods.*

3.3. A force-based quasi-continuum method. The force-based quasi-continuum (FQC) method differs from the previous methods by the fact that there does not exist an associated energy. One simple approach for constructing an FQC method is to keep (2.5) through (2.7) in the atomistic region, while the force balance equations computed from the CB rule are used in the continuum region. The resulting equilibrium equations are the same as (3.1) except that $(3.1)_2$ is valid up to $j = m$, and $(3.1)_3$ is valid from $j = m + 1$ to $j = n - 1$. In this case, we still have

$$u_m = u_{m+1} + P/\overline{\kappa}, \quad u_m = u_{m+2} + 2P/\overline{\kappa}. \tag{3.10}$$

Substituting the expression of u_j into the above equation, we obtain

$$(c, d)\mathcal{K}_{m+1} = -(\coth\delta, 1)(P/\overline{\kappa} + b). \tag{3.11}$$

Solving the above equations, we get

$$c = \frac{\sinh[m\delta]}{\sinh\delta}(P/\bar{\kappa} + b), \qquad d = -\frac{\cosh[m\delta]}{\sinh\delta}(P/\bar{\kappa} + b).$$

Copyright © by SIAM. Unauthorized reproduction of this article is prohibited.

Downloaded 02/26/15 to 124.16.148.3. Redistribution subject to SIAM license or copyright; see http://www.siam.org/journals/ojsa.php

Substituting the expressions of c and d into (2.19), we obtain

$$b = \frac{\mathcal{G}_{n-m,\alpha}(\delta)}{(1+\alpha)\sinh\delta - \mathcal{G}_{n-m,\alpha}(\delta)}\frac{P}{\overline{\kappa}} + \frac{(\alpha+\beta-1)\sinh\delta}{(1+\alpha)\sinh\delta - \mathcal{G}_{n-m,\alpha}(\delta)}u_n.$$

Finally, we substitute the expressions of b, c, and d into (2.18) and obtain

$$F(u_n) + \kappa^{\mathrm{fqc}}u_n + \eta^{\mathrm{fqc}}P = 0$$

with

$$\begin{aligned}\kappa^{\mathrm{fqc}} = (\alpha+\beta-1)&\left(\kappa_1 + \kappa_2(1+\beta) + \kappa_2\frac{\mathcal{G}_{n-m,1-\beta}(\delta)}{\mathcal{G}_{n-m,\alpha}(\delta) - (1+\alpha)\sinh\delta}\right)\\ &+ (\alpha+\beta-1)\frac{(\overline{\kappa}+(\beta-2)\kappa_2)\sinh\delta}{\mathcal{G}_{n-m,\alpha}(\delta) - (1+\alpha)\sinh\delta}\end{aligned}$$

and

$$\begin{aligned}\eta^{\mathrm{fqc}} = &\left(1 + \frac{(\beta-2)\kappa_2}{\overline{\kappa}}\right)\left(1 + \frac{(1+\alpha)\sinh\delta}{\mathcal{G}_{n-m,\alpha}(\delta) - (1+\alpha)\sinh\delta}\right)\\ &+ \frac{(1+\alpha)\kappa_2}{\overline{\kappa}}\frac{\mathcal{G}_{n-m,1-\beta}(\delta)}{\mathcal{G}_{n-m,\alpha}(\delta) - (1+\alpha)\sinh\delta}.\end{aligned}$$

We expand κ^{fqc} as follows:

$$\kappa^{\mathrm{fqc}} = \kappa_0 + 2(\alpha+\beta-1)\overline{\kappa}\frac{A_\alpha + B_\alpha - (\alpha+\beta-1)\sinh\delta}{(A_\alpha+B_\alpha)^2}z_0^{n-m} + \mathcal{O}(z_0^{2n-2m}).$$

We write η^{fqc} as

$$\eta^{\mathrm{fqc}} = 1 - \frac{(\alpha+\beta-1)\sinh[(n-m)\delta]}{\mathcal{G}_{n-m,\alpha}(\delta) - (1+\alpha)\sinh\delta} + \frac{(1+\alpha)\sinh\delta}{\mathcal{G}_{n-m,\alpha}(\delta) - (1+\alpha)\sinh\delta}.$$

Hence we have

$$\eta^{\mathrm{fqc}} = \eta_0 + \frac{(3+\alpha-\beta)\sinh\delta}{A_\alpha(\delta) + B_\alpha(\delta)}z_0^{n-m} + \mathcal{O}(z_0^{2n-2m}).$$

It is clear that $\kappa \to \kappa_0$ and $\eta \to \eta_0$ as $n - m \to \infty$.

3.4. A comparison test. As an example, we continue from the first numerical test and set $n = 104$. We computed the coefficients for $m = 99, 100, 101$, and 102. In Figure 6, the error in predicting the two parameters κ and η from the QC method is shown. We observe that the error in κ is quite small, and it is further reduced as m decreases (larger atomistic region). However, the error in η remains finite. We do not have a direct physical interpretation of this observation.

In Figure 7, the error from the QQC and FQC methods is shown. We observe that the error of both parameters for both methods converges exponentially. The QQC method offers faster convergence, which is consistent with our analysis.

4. Analysis of the bifurcation curves. Now we are ready to estimate the overall error, and we will focus on the error in u_n because the displacement of any other atoms can be expressed as a linear function of u_n, as shown in the previous section. The error for u_n is the error committed by solving the effective equations

Copyright © by SIAM. Unauthorized reproduction of this article is prohibited.

Downloaded 02/26/15 to 124.16.148.3. Redistribution subject to SIAM license or copyright; see http://www.siam.org/journals/ojsa.php

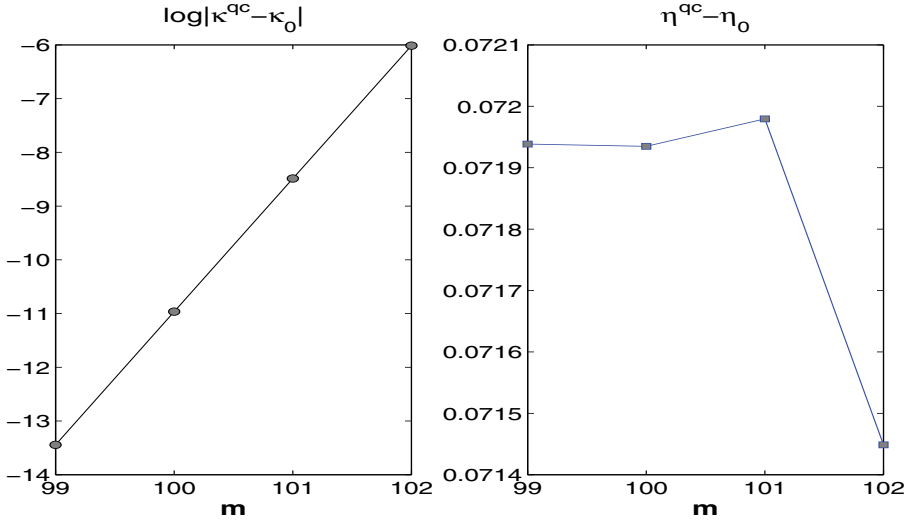

FIG. 6. *The error of the QC method without force correction. Left panel: The error in computing κ, shown on a log scale. Right panel: The error in η.*

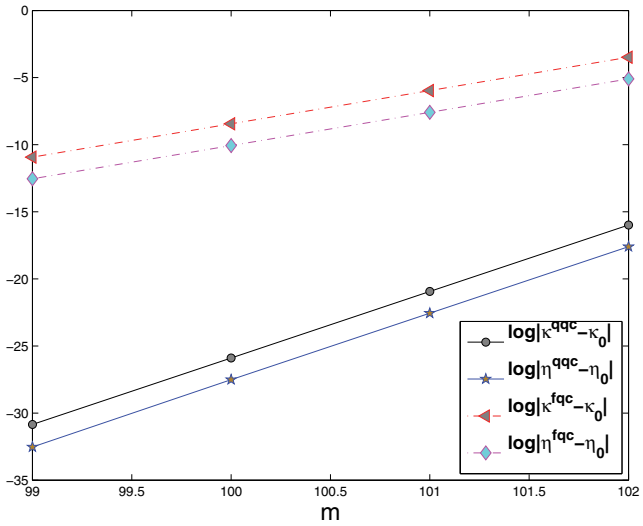

FIG. 7. *The error of the QQC and FQC methods (on a log scale).*

with the approximating parameters κ and η. It follows from Figures 4 and 5 that there might be multiple solutions of the effective equation with a given load P. In addition, there are two points when the derivative with respect to P is infinite. These two points are exactly the bifurcation points. Therefore, it is difficult to compare u_n with its approximations directly for the same loading parameter. In fact, we expect the error of u_n to be quite large near the bifurcation points.

Instead of a direct comparison, we propose a different approach, which is motivated by continuation methods for solving bifurcation problems [37, 38]. More specifically, we will compare the bifurcation curves as a whole. For this purpose,

Downloaded 02/26/15 to 124.16.148.3. Redistribution subject to SIAM license or copyright; see http://www.siam.org/journals/ojsa.php

Copyright © by SIAM. Unauthorized reproduction of this article is prohibited.

Downloaded 02/26/15 to 124.16.148.3. Redistribution subject to SIAM license or copyright; see http://www.siam.org/journals/ojsa.php

we parameterize the bifurcation curve on the $P-u$ plane using the arc length, which is denoted by s. Compared to the parameterization using the load parameter, the new representation is not multivalued. First we set the initial point of the curve to $(0,0)$, which clearly satisfies the effective equation for any choice of the parameters κ and η. Next we represent a point on the curve by $(P(s),u(s))$. To trace out the curve, one computes the tangent vector

$$\tau(s)=\big(f_1(u(s);\kappa,\eta),f_2(u(s);\kappa,\eta)\big),$$

where

$$f_1\big(u(s);\kappa,\eta\big)=-\frac{\eta}{\sqrt{(F'(u(s))+\kappa)^2+\eta^2}},\quad f_2\big(u(s);\kappa,\eta\big)=\frac{F'(u(s))+\kappa}{\sqrt{(F'(u(s))+\kappa)^2+\eta^2}}.$$

This can be easily obtained by differentiation of the effective equation with respect to the arc length. Following the curve with s as an independent variable, we obtain the following ODEs that describe the bifurcation curve [37]:

$$\begin{cases}\dfrac{d}{ds}u(s)=f_1\big(u(s);\kappa,\eta\big),\\[2mm]\dfrac{d}{ds}P(s)=f_2\big(u(s);\kappa,\eta\big),\\[2mm] \quad u(0)=0,\ P(0)=0.\end{cases}$$

As we have shown in the previous sections, a multiscale method typically gives an effective equation for u_n that is of the same form as the exact equation but with the approximate parameters κ and η. We denote the approximated values as $\widehat{\kappa}$ and $\widehat{\eta}$ and the corresponding bifurcation curve as $\big(\widehat{P}(s),\widehat{u}(s)\big)$, respectively. We can describe the bifurcation curve by the following ODEs:

$$\begin{cases}\dfrac{d}{ds}\widehat{u}(s)=f_1\big(\widehat{u}(s);\widehat{\kappa},\widehat{\eta}\big),\\[2mm]\dfrac{d}{ds}\widehat{P}(s)=f_2\big(\widehat{u}(s);\widehat{\kappa},\widehat{\eta}\big),\\[2mm] \quad \widehat{u}(0)=0,\ \widehat{P}(0)=0.\end{cases}$$

In this way, the problem has been reduced to a perturbation problem with varying parameters. Standard theory for ODEs states that the solution is continuously dependent on the parameters [35], provided that the functions f_1 and f_2 are Lipschitz continuous. This can be explicitly stated as follows. For any $s\in[0,S]$,

$$|u(s)-\widehat{u}(s)|+|P(s)-\widehat{P}(s)|\le L\left(|\kappa-\widehat{\kappa}|+|\eta-\widehat{\eta}|\right)e^{LS},$$

where L is the Lipschitz constant of f_1 and f_2. In particular, the error in u_n will depend continuously on the parameters κ and η, and for the QQC and the FQC methods, this error should be exponentially small. More importantly, this estimate is not restricted to a local minimum.

One remaining issue is estimating the error in the continuum region. For the current problem, once u_n is obtained from the bifurcation diagram, the rest of the degrees of freedom are uniquely determined. This makes it possible to interpret the error in the continuum region. In the context of bifurcation theory, the effective equation (2.20) describes a center manifold, where the transition occurs. The remaining

Copyright © by SIAM. Unauthorized reproduction of this article is prohibited.

Downloaded 02/26/15 to 124.16.148.3. Redistribution subject to SIAM license or copyright; see http://www.siam.org/journals/ojsa.php

degrees of freedom lie in the stable manifold, and standard methods in numerical analysis may apply. This issue for more general problems will be addressed in future works.

Appendix A. Derivation of equations (3.6). We first introduce a shorthand notation. For $a, x \in \mathbb{R}$, denote

$$s_a(x) = \sinh[ax], \quad c_a(x) = \cosh[ax].$$

Proof of (2.16) *and* (2.17). The identity (2.16) is equivalent to

$$\kappa_2 \left(c_{k+1}(\delta) - c_{k-2}(\delta)\right) + (\kappa_1 + \kappa_2)\left(c_k(\delta) - c_{k-1}(\delta)\right) = 0.$$

The left-hand side of the above equation can be written as

$$2s_{k-1/2}(\delta)\left(\kappa_2 s_{3/2}(\delta) + (\kappa_1 + \kappa_2)s_{1/2}(\delta)\right).$$

Using (2.14), we obtain

$$\kappa_2 s_{3/2}(\delta) + (\kappa_1 + \kappa_2)s_{1/2}(\delta) = s_{1/2}(\delta)\left(\kappa_2(2c_1(\delta) + 1) + \kappa_1 + \kappa_2\right) = 0.$$

This completes the proof for (2.16).

We omit the proof for (2.17) since it is the same. □

To derive (3.6), we first substitute (3.5) into $(3.4)_2$ and obtain

$$\begin{aligned}
&\Big\{(\kappa_1 + \kappa_2)\left(c_{m+2}(\delta) - c_{m+1}(\delta)\right) + \kappa_2\left(c_{m+3}(\delta) - c_{m+1}(\delta)\right)\Big\}c \\
&+ \Big\{(\kappa_1 + \kappa_2)\left(s_{m+2}(\delta) - s_{m+1}(\delta)\right) + \kappa_2\left(s_{m+3}(\delta) - s_{m+1}(\delta)\right)\Big\}d \\
&= -P - (\kappa_1 + 3\kappa_2)b.
\end{aligned}$$

Using (2.16) and (2.17) with $k = m + 2$ to simplify the coefficients for c and d, respectively, we obtain a simplified form of $(3.4)_2$ as

$$\big(c_{m+1}(\delta) - c_m(\delta)\big)c + \big(s_{m+1}(\delta) - s_m(\delta)\big)d = \frac{P}{\kappa_2} + \frac{\kappa_1 + 3\kappa_2}{\kappa_2}b. \tag{A.1}$$

Next we substitute (3.5) into $(3.4)_1$ and obtain

$$\begin{aligned}
&\Big\{(\kappa_1 + \gamma\kappa_2/2)\left(c_{m+1}(\delta) - c_m(\delta)\right) + \kappa_2\left(c_{m+2}(\delta) - c_m(\delta)\right)\Big\}c \\
&+ \Big\{(\kappa_1 + \gamma\kappa_2/2)\left(s_{m+1}(\delta) - s_m(\delta)\right) + \kappa_2\left(s_{m+2}(\delta) - s_m(\delta)\right)\Big\}d \\
&+ (\kappa_1 + (\gamma/2 + 2)\kappa_2)\, b = -\gamma P.
\end{aligned} \tag{A.2}$$

A direct calculation yields

$$\begin{aligned}
\kappa_1\left(c_{m+1}(\delta) - c_m(\delta)\right) + \kappa_2\left(c_{m+2}(\delta) - c_m(\delta)\right) &= -2\kappa_2 s_1(\delta)s_m(\delta), \\
\kappa_1\left(s_{m+1}(\delta) - s_m(\delta)\right) + \kappa_2\left(s_{m+2}(\delta) - s_m(\delta)\right) &= -2\kappa_2 s_1(\delta)c_m(\delta).
\end{aligned}$$

Using the above two equations, we may write (A.2) as

$$\begin{aligned}
&\Big(\frac{\gamma}{2}[c_{m+1}(\delta) - c_m(\delta)] - 2s_1(\delta)s_m(\delta)\Big)\, c + \Big(\frac{\gamma}{2}[s_{m+1}(\delta) - s_m(\delta)] - 2s_1(\delta)c_m(\delta)\Big)\, d \\
&= -\frac{\gamma}{\kappa_2}P - \frac{\kappa_1 + (\gamma/2 + 2)\kappa_2}{\kappa_2}b.
\end{aligned}$$

Copyright © by SIAM. Unauthorized reproduction of this article is prohibited.

Downloaded 02/26/15 to 124.16.148.3. Redistribution subject to SIAM license or copyright; see http://www.siam.org/journals/ojsa.php

Using (A.1), we simplify the above equation into

$$s_m(\delta)c + c_m(\delta)d = \frac{3\gamma}{4\kappa_2 \sinh\delta}P + \frac{(\gamma+2)\overline{\kappa} - 4\kappa_2}{4\kappa_2 \sinh\delta}b.$$

This gives the first equation in (3.6), which together with (A.2) yields the second equation in (3.6).

Appendix B. Derivation of (3.9). To derive (3.9), we first substitute the expression of u_j into (3.8) and obtain

$$\begin{aligned}&\big((\kappa_1+2\kappa_2)(c_m(\delta)-c_{m-1}(\delta)) + \kappa_2(c_{m+1}(\delta)-c_{m-1}(\delta))\big)c\\ &+\big((\kappa_1+2\kappa_2)(s_m(\delta)-s_{m-1}(\delta)) + \kappa_2(s_{m+1}(\delta)-s_{m-1}(\delta))\big)d = -P - \overline{\kappa}b\end{aligned}$$

and

$$\begin{aligned}&\Big\{-(\kappa_1+2\kappa_2)(c_m(\delta)-c_{m-1}(\delta))\\ &\quad+\kappa_1(c_{m+1}(\delta)-c_m(\delta)) + \kappa_2(c_{m+2}(\delta)-c_m(\delta))\Big\}c\\ &+\Big\{-(\kappa_1+2\kappa_2)(s_m(\delta)-s_{m-1}(\delta))\\ &\quad+\kappa_1(s_{m+1}(\delta)-s_m(\delta)) + \kappa_2(s_{m+2}(\delta)-s_m(\delta))\Big\}d = 0.\end{aligned}$$

Using (2.14), we obtain

$$\begin{aligned}&(\kappa_1+2\kappa_2)(c_m(\delta)-c_{m-1}(\delta)) + \kappa_2(c_{m+1}(\delta)-c_{m-1}(\delta))\\ &\qquad= (\kappa_1+2\kappa_2+2(\cosh\delta+1)\kappa_2)(\cosh\delta-1)c_{m-1}(\delta)\\ &\qquad\quad+(\kappa_1+2\kappa_2+2\kappa_2\cosh\delta)s_1(\delta)s_{m-1}(\delta)\\ &\qquad= -\overline{\kappa}c_{m-1}(\delta).\end{aligned} \tag{B.1}$$

Proceeding along the same line that leads to the above identity, we have

$$(\kappa_1+2\kappa_2)(s_m(\delta)-s_{m-1}(\delta)) + \kappa_2(s_{m+1}(\delta)-s_{m-1}(\delta)) = -\overline{\kappa}s_{m-1}(\delta).$$

Using (B.1), we write

$$\begin{aligned}&-(\kappa_1+2\kappa_2)(c_m(\delta)-c_{m-1}(\delta)) + \kappa_1(c_{m+1}(\delta)-c_m(\delta)) + \kappa_2(c_{m+2}(\delta)-c_m(\delta))\\ &= -\big\{(\kappa_1+2\kappa_2)(c_m(\delta)-c_{m-1}(\delta)) + \kappa_2(c_{m+1}(\delta)-c_{m-1}(\delta))\big\}\\ &\quad+\big\{(\kappa_1+\kappa_2)(c_{m+1}(\delta)-c_m(\delta)) + \kappa_2(c_{m+2}(\delta)-c_{m-1}(\delta))\big\}\\ &= \overline{\kappa}c_{m-1}(\delta),\end{aligned}$$

where we have used (2.16) with $k = m+1$ in the last step.

Proceeding along the same line that leads to the above identity, we obtain

$$-(\kappa_1+2\kappa_2)(s_m(\delta)-s_{m-1}(\delta)) + \kappa_1(s_{m+1}(\delta)-s_m(\delta)) + \kappa_2(s_{m+2}(\delta)-s_m(\delta)) = \overline{\kappa}s_{m-1}(\delta).$$

Combining the above two equations, we obtain (3.9).

Appendix C. Derivation of (3.11). To derive (3.11), we substitute the expression of u_j into (3.10) and obtain

$$\begin{cases}\big(c_{m+1}(\delta)-c_m(\delta)\big)c + \big(s_{m+1}(\delta)-s_m(\delta)\big)d = -P/\overline{\kappa},\\ \big(\kappa_1(c_{m+2}(\delta)-c_{m+1}(\delta)) + \kappa_2(c_{m+3}(\delta)-c_{m+1}(\delta))\big)c\\ +\big(\kappa_1(s_{m+2}(\delta)-s_{m+1}(\delta)) + \kappa_2(s_{m+3}(\delta)-s_{m+1}(\delta))\big)d\\ = -(\kappa_1+2\kappa_2)(P/\overline{\kappa}+b).\end{cases}$$

Copyright © by SIAM. Unauthorized reproduction of this article is prohibited.

Downloaded 02/26/15 to 124.16.148.3. Redistribution subject to SIAM license or copyright; see http://www.siam.org/journals/ojsa.php

Proceeding along the same line that leads to (B.1), we obtain

$$\kappa_1 \left(c_{m+2}(\delta) - c_{m+1}(\delta)\right) + \kappa_2 \left(c_{m+3}(\delta) - c_{m+1}(\delta)\right) = -2\kappa_2 s_1(\delta) s_{m+1}(\delta),$$
$$\kappa_1 \left(s_{m+2}(\delta) - s_{m+1}(\delta)\right) + \kappa_2 \left(s_{m+3}(\delta) - s_{m+1}(\delta)\right) = -2\kappa_2 s_1(\delta) c_{m+1}(\delta).$$

We write the second equation of the coupling conditions as

$$s_{m+1}(\delta)c + c_{m+1}(\delta)d = \frac{\kappa_1 + 2\kappa_2}{2\kappa_2 \sinh\delta}(P/\bar{\kappa} + b) = -\coth\delta(P/\bar{\kappa} + b).$$

This gives the first equation in (3.11).

In addition, we can write the first equation of the coupling equations as

$$\big(c_{m+1}(\delta)c + s_{m+1}(\delta)d\big)(1 - \cosh\delta) + \big(s_{m+1}(\delta)c + c_{m+1}(\delta)d\big)\sinh\delta = -P/\bar{\kappa} - b,$$

which together with the first equation in (3.11) implies the second equation in (3.11).

REFERENCES

[1] T. Belytschko and S.P. Xiao, *Coupling methods for continuum model with molecular model*, Int. J. Multiscale Comput. Eng., 1 (2003), pp. 115–126.

[2] É. Benoît, *Dynamic Bifurcations*, Springer-Verlag, Berlin, 1991.

[3] M. Born and K. Huang, *Dynamical Theory of Crystal Lattices*, Oxford University Press, New York, 1954.

[4] J. Carr, *Applications of Centre Manifold Theory*, Springer-Verlag, New York, 1981.

[5] J.R. Chen and P.B. Ming, *Ghost force influence of a quasicontinuum method in two dimension*, J. Comput. Math., 30 (2012), pp. 657–683.

[6] K.S. Cheung and S. Yip, *A molecular-dynamics simulation of crack-tip extension: The brittle-to-ductile transition*, Model. Simulat. Mater. Sci. Eng., 2 (1994), pp. 865–892.

[7] S.-N. Chow and J.K. Hale, *Methods of Bifurcation Theory*, Springer-Verlag, New York, Berlin, 1982.

[8] B. Cotterell and J.R. Rice, *Slightly curved or kinked cracks*, Int. J. Fracture, 16 (1980), pp. 155–169.

[9] L. Cui and P.B. Ming, *The effect of ghost forces for a quasicontinuum method in three dimension*, Sci. China Math., 56 (2013), pp. 2571–2589.

[10] M. Dobson and M. Luskin, *An analysis of the effect of ghost force oscillation on quasicontinuum error*, M2AN Math. Model. Numer. Anal., 43 (2009), pp. 591–604.

[11] M. Dobson and M. Luskin, *An optimal order error analysis of the one-dimensional quasicontinuum approximation*, SIAM J. Numer. Anal., 47 (2009), pp. 2455–2475.

[12] M. Dobson, M. Luskin, and C. Ortner, *Accuracy of quasicontinuum approximations near instabilities*, J. Mech. Phys. Solids, 58 (2010), pp. 1741–1757.

[13] M. Dobson, M. Luskin, and C. Ortner, *Sharp stability estimates for the force-based quasicontinuum approximation of homogeneous tensile deformation*, Multiscale Model. Simul., 8 (2010), pp. 782–802.

[14] M. Dobson, M. Luskin, and C. Ortner, *Stability, instability, and error of the force-based quasicontinuum approximation*, Arch. Ration. Mech. Anal., 197 (2010), pp. 179–202.

[15] W. E, J. Lu, and J.Z. Yang, *Uniform accuracy of the quasicontinuum method*, Phys. Rev. B, 74 (2006), 214115.

[16] W. E and P.B. Ming, *Analysis of the local quasicontinuum methods*, in Frontiers and Prospects of Contemporary Applied Mathematics, T. Li and P.W. Zhang, eds., Higher Education Press, Beijing, World Scientific, Singapore, 2005, pp. 18–32.

[17] R.S. Elliott, J.A. Shaw, and N. Triantafyllidis, *Stability of thermally-induced martensitic transformations in bi-atomic crystals*, J. Mech. Phys. Solids, 50 (2002), pp. 2463–2493.

[18] E.R. Fuller and R.M. Thomson, *Lattice theories of fracture*, in Fracture Mechanics of Ceramics, Vol. 4, Plenum Press, New York, 1978, pp. 507–548.

[19] J. Guckenheimer and P. Holmes, *Nonlinear Oscillations, Dynamical Systems, and Bifurcations of Vector Fields*, Springer-Verlag, New York, 1983.

[20] V. Jusuf, *Algorithms for Branch-Following and Critical Point Identification in the Presence of Symmetry*, Ph.D. thesis, University of Minnesota, Minneapolis, MN, 2010.

Copyright © by SIAM. Unauthorized reproduction of this article is prohibited.

[21] J. Knap and M. Ortiz, *An analysis of the quasicontinuum method*, J. Mech. Phys. Solids, 49 (2001), pp. 1899–1923.
[22] X. Li, *An atomistic-based boundary element method for the reduction of the molecular statics models*, Comput. Methods Appl. Mech. Engrg., 225 (2012), pp. 1–13.
[23] X. Li, *A bifurcation study of crack initiation and kinking*, Eur. Phys. J. B, 86 (2013), 258.
[24] X. Li, *Dynamic Crack Initiation through Bifurcation*, preprint, 2014.
[25] X. Li and P.B. Ming, *On the effect of ghost force in the quasicontinuum method: Dynamic problems in one dimension*, Commun. Comput. Phys., 15 (2014), pp. 647–676.
[26] P. Lin, *Theoretical and numerical analysis for the quasi-continuum approximation of a material particle model*, Math. Comp., 72 (2003), pp. 657–675.
[27] J. Lu and P.B. Ming, *Convergence of a force-based hybrid method in three dimensions*, Comm. Pure Appl. Math., 66 (2013), pp. 83–108.
[28] T. Ma and S. Wang, *Bifurcation Theory and Applications*, World Scientific, Hackensack, NJ, 2005.
[29] J.E. Marsden and T.J.R. Hughes, *Mathematical Foundations of Elasticity*, Dover, New York, 1994.
[30] P.B. Ming, *Error estimate of force-based quasicontinuum method*, Commun. Math. Sci., 6 (2008), pp. 1087–1095.
[31] P. Ming and J.Z. Yang, *Analysis of a one-dimensional nonlocal quasi-continuum method*, Multiscale Model. Simul., 7 (2009), pp. 1838–1875.
[32] C. Ortner, *The role of the patch test in 2d atomistic-to-continuum coupling methods*, ESAIM Math. Model. Numer. Anal., 46 (2012), pp. 1275–1319.
[33] C. Ortner and A.V. Shapeev, *Analysis of an energy-based atomistic/continuum coupling approximation of a vacancy in the 2d triangular lattice*, Math. Comp., 82 (2013), pp. 2191–2236.
[34] C. Ortner and E. Süli, *Analysis of a quasicontinuum method in one dimension*, ESAIM Math. Model. Numer. Anal., 42 (2008), pp. 57–91.
[35] L. Perko, *Differential Equations and Dynamical Systems*, 3rd ed., Springer-Verlag, New York, 2001.
[36] I. Plans, A. Carpio, and L.L. Bonilla, *Homogeneous nucleation of dislocations as bifurcations in a periodized discrete elasticity model*, Eur. Phys. J. B, 81 (2008), 36001.
[37] W.C. Rheinboldt and J.V. Burkardt, *A locally parameterized continuation process*, ACM Trans. Math. Software, 9 (1983), pp. 215–235.
[38] R. Seydel, *Practical Bifurcation and Stability Analysis*, 3rd ed., Springer, New York, 2010.
[39] A.V. Shapeev, *Consistent energy-based atomistic/continuum coupling for two-body potentials in one and two dimensions*, Multiscale Model. Simul., 9 (2011), pp. 905–932.
[40] T. Shimokawa, J.J. Mortensen, J. Schioz, and K.W. Jacobsen, *Matching conditions in the quasicontinuum method: Removal of the error introduced at the interface between the coarse-grained and fully atomistic region*, Phys. Rev. B, 69 (2004), 214104.
[41] J. Sotomayor, *Generic bifurcation of dynamical system*, in Dynamical Systems, M.M. Peixoto, ed., Academic Press, New York, 1973, pp. 561–582.
[42] E.B. Tadmor, M. Ortiz, and R. Phillips, *Quasicontinuum analysis of defects in solids*, Philos. Mag. A, 73 (1996), pp. 1529–1563.
[43] R. Thompson, C. Hsieh, and V. Rana, *Lattice trapping of fracture cracks*, J. Appl. Phys., 42 (1971), pp. 3154–3160.
[44] G.J. Wagner and W.K. Liu, *Coupling of atomistic and continuum simulations using a bridging scale decomposition*, J. Comput. Phys., 190 (2003), pp. 249–274.

Downloaded 02/26/15 to 124.16.148.3. Redistribution subject to SIAM license or copyright; see http://www.siam.org/journals/ojsa.php

Copyright © by SIAM. Unauthorized reproduction of this article is prohibited.